Global Positioning System constraints on fault slip rates in the Death Valley region, California and Nevada.

R. A. Bennett & J. L. Davis
Harvard-Smithsonian Center for Astrophysics, Cambridge, MA

P. Elósegui
Harvard-Smithsonian Center for Astrophysics, Cambridge, MA and Institut d'Estudis Especials de Catalunya, Barcelona, Spain

B. P. Wernicke, J.K. Snow, M.J. Abolins & M.A. House
California Institute of Technology, Pasadena, CA

G. L. Stirewalt & D. A. Ferrill
Center for Nuclear Waste Regulatory Analyses. San Antonio, TX

Received _____; accepted _____

Abstract. We estimated the horizontal velocities at 15 locations in the vicinity of Yucca Mountain, Nevada, from Global Positioning System (GPS) surveys conducted between 1991 and 1996. We used these velocity estimates to infer slip rates on two major Quaternary faults within the ECSZ, the Hunter Mountain and Death Valley faults. The sum of slip rates across the two faults is well determined at 5 ± 1 mm/yr (one standard deviation). Between 3 to 5 mm/yr of this motion appears to be accommodated along the Death Valley fault, implying 30-50 m of strain accumulation over the next 10,000 yr. If so, there is potential for 5 to 10 M_w 6.5-7.5 earthquakes during this period, consistent with paleoseismological studies of the fault zone. Yucca Mountain, which lies 50 km east of the eastern California shear zone (ECSZ), is the proposed location for the disposal of high-level nuclear waste in the United States.

Introduction

Between 9% and 23% of modern Pacific-North America relative plate motion is transferred from the Salton Trough of southern California to the Basin and Range Province of the western United States by means of the eastern California shear zone (ECSZ) [*Sauber et al.*, 1994] (Figure 1). The contemporary distribution of deformation within the ECSZ has important implications for the long term accumulation and release of strain in the continental crust and bears directly on the reliability of paleoseismological inferences for assessing seismic risk. Although much has been learned about the ECSZ through geological observations and conventional terrestrial and space geodetic measurements, the distribution of strain accumulation at latitude $\sim$ 37°N is not yet well constrained. A better understanding of this deformation is critical, as Yucca Mountain, Nevada, the proposed disposal site for high-level nuclear waste in the United States, lies only 50 km to the east.

At latitude 37°N, the ECSZ is expressed mainly as three right-lateral, locally transtensional fault zones, including the Death Valley-Furnace Creek (DVFC), Hunter Mountain-Panamint Valley (HMPV), and Owens Valley (OVFZ) fault zones (Figure 1). Geological evidence indicates that since 5 Ma the ECSZ accommodated $\sim$ 10 mm/yr of right-lateral displacement across these faults [*Wernicke et al.*, 1988; *Dokka and Travis*, 1990]. Paleoseismological data, representing Quaternary strain release, indicate that the DVFC fault zone and its northern extension, the Fish Lake Valley fault zone, accommodated 4–6 mm/yr or more of right-lateral motion [*Brogen et al.*, 1991; *Dixon et al.*, 1995; *Reheis and Sawyer*, 1997]. Somewhat smaller slip rates are estimated for the HMPV fault zone (2.4 $\pm$ 0.8 mm/yr) [*Zhang et al.*, 1990] and for the OVFZ and its northern extension, the White Mountains fault zone (0.5–2.0 mm/yr) [*dePolo*, 1989; *Beanland and Clark*, 1995].

At latitude 34.5°N, the ECSZ manifests itself within Mojave Desert terrestrial geodetic networks as an apparent right-lateral northwest shear of as much as 12 mm/yr extending northward into Owens Valley [*Sauber et al.*, 1994]. Deformation within this network attenuates rapidly eastward [e.g., *Sauber et al.*, 1986]. At latitude 37°N, there is no evidence for deformation of greater than about 2 mm/yr across the Yucca Mountain trilateration network [*Savage et al.*, 1994]. Deformation within the Owens Valley trilateration network, to the west, accounts for up to 7 mm/yr of right-lateral slip on the OVFZ fault [*Savage and Lisowski*, 1995]. These results suggest that present-day strain accumulation at 37°N may be concentrated along the western margin of the ECSZ, in contrast to the paleoseismological data which indicate concentration of strain toward the east. Several models have been formulated to reconcile the discrepancy between these observations, all involving westward migration of shear strain within the ECSZ over the last few million years [e.g., *Dokka and Travis*, 1990; *Savage and Lisowski*,

1995; *Dixon et al.*, 1995].

Previous space geodetic observations provide limited additional constraints. The relative motion between sites straddling the San Andreas and western Mojave (VNDN and MOJA, Figure 1) is accurately determined (38.5 ± 0.2 mm/yr) [*Feigl et al.*, 1993]. The distribution of this motion among the greater San Andreas fault system and faults of the ECSZ in the central Mojave, however, is not yet clear. The velocity of site MOJA with respect to stable north America (8.4 ± 0.2 mm/yr [c.f., *Feigl et al.*, 1993]), provides an upper bound on the total ECSZ deformation to the east, which presumably includes the HMPV and DVFC fault zones.

In this paper, we analyze Global Positioning System (GPS) observations collected over the last five years to investigate the distribution and sum of contemporary deformation along the portion of the ECSZ east of Owens Valley and in the vicinity of Yucca Mountain. We reserve a detailed discussion of deformation in the direct vicinity of Yucca Mountain for a future publication.

GPS Observations

Between 1991 and 1996, we conducted five GPS surveys within and around the ECSZ in the vicinity of Yucca Mountain, Nevada. The network consists of 15 stations, comprising three subnetworks and two additional sites (Figures 1 and 2). We analyzed these data using the GAMIT/GLOBK software [*King and Bock*, 1995; *Herring*, 1995]. In our analyses, we included all available global tracking data from the International GPS Service for Geodynamics (IGS) and made use of data products provided by the Scripps Orbit and Permanent Array Center (SOPAC).

We first investigated the extent to which our velocity estimates were affected by coseismic displacements associated with the 1992 M_s 7.5 Landers and M_s 5.4 Little Skull Mountain earthquakes (Figure 1). We compared velocity estimates resulting from solutions with and without earthquake displacement parameters employed, and found no significant differences. Site velocities are determined primarily by the more accurate, 1993-1996 surveys. The data are not sensitive to these earthquakes due to the rather large uncertainties in the positions estimated from the 1991 survey relative to the expected coseismic deformation [*Hudnut et al.*, 1994; *Savage et al.*, 1994]. Given these uncertainties, our data set provides a loose upper bound on the earthquake displacements of 8 mm at the 95% confidence level. The largest horizontal displacements, calculated using the Little Skull Mountain dislocation model of *Savage et al.* [1994], occur at sites 67TJ (7 mm), BLC1 (3 mm), MILE (5 mm), and WAHO (3 mm) in the Yucca Mountain subnetwork.

We show our velocity estimates computed with respect to site BLC1 in Figure 2 (with 95%

confidence ellipses), and list these estimates in Table 1 (with one standard deviation uncertainties). Figure 3 shows the time evolution of the LEEF-BLC1 baseline, one of the longest baselines in the network. The average weighted root-mean-square scatters in the components of the residual baseline estimates (removing the trend derived from the rate estimates) are 2, 2, 9, and 2 mm in the north, east, up, and length components, respectively. The corresponding χ^2 per degree of freedom values for all baseline components are near 1.0, indicating that the formal uncertainties are consistent with the scatter in the data. Vertical velocity estimates are significant at the 95% confidence level for only three sites (DANT, GRAP, WAHO; Table 1).

From the horizontal velocity estimates we make the following observations: The total deformation across the network west of BLC1 (relative motion between sites BLC1 and LEEF) is 4.0 ± 0.5 mm/yr (one standard deviation). Deformation within the network is dominated by right-lateral northwest trending shear with steepest gradients over the DVFC fault zone. The exception to this general pattern is site AGUE which exhibits a large component of motion perpendicular to the average direction of shear. Deformation among sites in the Yucca Mountain subnetwork is small, consistent with the results of *Savage et al.* [1994].

Dislocation Model

We followed the modeling and inversion approach of *Bennett et al.* [1996] to eliminate the dependence of our modeling results on possible GPS reference frame biases. The eastern ECSZ within the span of our network was modeled as a set of elastic blocks bounded by planar, infinite, parallel dislocations representing, from east to west, the DVFC, HMPV, and OVFZ fault zones (Figure 4). The faults were assumed to be locked to 15 km depth. Model velocities were computed from a superposition of relative, rigid body motions and the elastic deformation field induced by the locked, near surface parts of the faults. We constrained the azimuth of relative block motions to be equal to that of the dislocation planes (320°).

Using the horizontal components of our GPS velocity estimates and their error covariance matrix, we estimated slip rates on the three model faults. Because our model is one dimensional, we did not use the velocities at sites DANT and AGUE, as these sites lie close to a major right stepping jog in the DVFC fault zone. We achieved a χ^2 value of 124, yielding a χ^2 per degree of freedom of about 6. The residual velocity field is shown in Figure 4 and the resulting slip rate estimates are listed in Table 2 (solution 1). As described by *Bennett et al.* [1996], we have estimated a horizontal translation between the model predictions and the observed velocities. Consequently we are concerned only with

the components of the velocity field that cannot be explained by a systematic translation. Hence we compare the residual velocity field to the confidence ellipses derived from a projected version of the original covariance matrix.

As expected, the OVFZ slip rate is very poorly resolved (solution 1, Table 2). Therefore, we re-estimated the DVFC and HMPV slip rates in two solutions wherein the OVFZ fault slip rate was constrained to the values of 0 mm/yr and 7 mm/yr (solutions 2 and 3), respectively. We found that the estimates for the DVFC and HMPV slip rates are unaffected at the one standard deviation level and that the increase in the sum of squared residuals was insignificant for both cases. We performed a similar numerical experiment wherein the HMPV fault slip rate was constrained to zero (solution 4) with similar results. In this solution, the slip rate estimate for the DVFC fault accommodates all of the motion within the network; it is equal to the sum of the DVFC and HMPV slip rate estimates of the previous solutions. Finally, we estimated the HMPV and OVFZ slip rates under the hypothesis that the DVFC slip rate is zero (solution 5). We may reject this hypothesis given our data and model with greater than 98% confidence. Based on our data and these tests, we cannot reject with sufficient confidence models in which the slip rate on either the HMPV or OVFZ fault is constrained to be zero. The DVFC slip rate estimate resulting when both these slip rates are constrained to zero (solution 6) is large and well determined (5±1 mm/yr).

We then tested the sensitivity of the velocity estimates to the locking depths of the DVFC and HMPV faults. We performed four additional solutions using the parameterization of solution 6 but with the locking depth of the DVFC fault set to 10, 13, 17 and 20 km. The resulting DVFC fault slip rate estimates are constant and equal to that of solution 6 to within their uncertainties. Geological evidence suggests that the locking depth of the HMPV fault zone may be very shallow [Burchfiel et al., 1987]. Estimating the slip rates on all three fault systems, under the assumption of a 5 km locking depth for the HMPV fault, yields marginally smaller rates for all faults with slightly smaller uncertainties.

We have chosen the strike of the fault systems based on the general trend of the surface traces of the faults. Because these traces are clearly not linear, we tested the sensitivity of our results to the value of the strike adopted. We found no significant variation in the results through the range 310-330°.

Finally, we tested a solution wherein we constrained the values of the OVFZ and HMPV fault slip rates to their paleoseismological estimates of 2.0 ± 0.5 and 2.4 ± 0.8 mm/yr, respectively [*Beanland and Clark*, 1995; *Zhang et al.*, 1990]. The estimate that we obtain for the DVFC fault of 3 ± 1 mm/yr (solution 7) differs insignificantly from the paleoseismological estimates of 4–6 mm/yr [e.g., *Reheis and Sawyer*, 1997].

Discussion and Conclusion

We analyzed five epochs of GPS data collected along the eastern edge of the ECSZ in the vicinity of Yucca Mountain, Nevada. The site velocities that we infer from these data are not sensitive to coseismic deformation associated with the 1992 Landers and Little Skull Mountain earthquakes. The data provide a loose upper bound on horizontal deformation associated with these events (at our sites) to be less than about 8 mm at the 95% confidence level.

The general pattern of deformation that we observe is predominantly right-lateral shear. Using a simple, one dimensional, elastic block model, we inferred slip rates on the Death Valley fault in the range of 3–5 mm/yr depending on the slip rate of the Hunter Mountain fault. The sum of deformation across the network is well determined, however, at about 5 ± 1 mm/yr (one standard deviation). Within error, our slip rate estimates are consistent with rates suggested by *Dixon et al.* [1995]. An additional measurement of this integrated deformation across our network resulted from our GPS analyses; we estimated a rate of 5.1 ± 0.7 mm/yr relative motion between sites DS10 (part of the IGS network) and BLC1 (Figure 2). DS10 is located roughly 10 km north of site MOJA (Figures 1 and 2). Both of these sites lie well east of the southern extrapolation of the OVFZ fault zone, but west of the extrapolations of the HMPV and DVFC fault zones. Although the applicability of our simple model is questionable south of the Garlock fault, we found that the north and east components of the difference between our velocity estimate for site DS10 and the velocity predicted by our model (in the projected, no-net-translation frame of reference) are insignificant at 0.1 ± 0.4 and -0.3 ± 0.3 mm/yr, respectively (Figure 4).

We cannot distinguish between 0 and 7 mm/yr slip rate on the Owens Valley fault with our data set. Similarly, we provide only very loose constraints on the slip rate of the Hunter Mountain fault (± 3 mm/yr). However, our velocity field is consistent with paleoseismological estimates of slip rate within these fault zones and with other geodetic and geological observations. Although evidence from previous studies discussed above suggests a general westward shift of deformation across the three fault zones in the region with time, our results suggest that substantial active shear (3–5 of the total 6–12 mm/yr) is concentrated on the eastern portion of the ECSZ.

Paleoseismological analyses of the Death Valley fault zone indicate that 4-6 separate moderate to large (M > 6.5) earthquakes have occurred along various segments of the fault since 10 ka [e.g., *Brogen et al.*, 1991]. Given the 3-5 mm/yr slip rate that we infer for the Death Valley fault, we may expect 5-10 M_W 6.5-7.5 earthquakes to occur over the next ten thousand years.

Acknowledgments. This project was supported by NRC Contracts NRC-04-92-071 and NRC-02-93-005, NSF Grant EAR-94-18784, and the Smithsonian Institution. The views and conclusions expressed in this paper do not represent an official regulatory position of the United States Nuclear Regulatory Commission (NRC). This manuscript benefited from careful reviews by Eugene Humphreys, Richard Snay, and an anonymous referee. We also wish to thank Jim Savage for useful discussions. We made extensive use of GPS data products provided by the Scripps Orbit and Permanent Array Center.

References

Beanland, S. and M. M. Clark, The Owens Valley fault zone, eastern California, and surface rupture associated with th 1872 earthquake, *U.S. Geol. Sur. Bull., 1892,* 1995.

Bennett, R. A. , W. Rodi, and R. E. Reilinger, Global Positioning System constraints on fault slip rates in southern California and northern Baja, Mexico, *J. Geophys. Res., 101,* 21,943–21,960, 1996.

Brogen, G. E. , K. S. Kellog, D. B. Slemmons, and C. Terhune, Late Quaternary faulting along the Death Valley-Furnace Creek fault system, California and Nevada, *U.S. Geol. Surv. Bull., 1991,* 23 pp., 1991.

Burchfiel, B. C. , K. V. Hodges, and L. H. Royden, Geology of Panamint Valley – Saline Valley pull-apart system, California: Palinspastic evidence for low-angle geometry of a Neogene range-bounding fault, *J. Geophys. Res., 91,* 10,422–10,426, 1987.

dePolo, C. M. , *Seismotectonics of the White Mountains fault system, east-central California, and west-central Nevada,* PhD thesis, University of Nevada, Reno, 1989.

Dixon, T. H. , R. Stefano, J. Lee, and M. C. Reheis, Constraints on present-day Basin and Range deformation from space geodesy, *Tectonics, 14,* 755–772, 1995.

Dokka, R. K. and C. J. Travis, Role of the eastern California shear zone in accommodating Pacific-North American plate motion, *Geophys. Res. Lett., 17,* 1323–1326, 1990.

Feigl, K. L. , D. C. Agnew, Y. Bock, D. Dong, A. Donnellan, B. H. Hager, T. A. Herring, D. D. Jackson, T. H. Jordan, R. W. King, S. Larsen, K. M. Larson, M. H. Murray, Z. Shen, and F. H. Webb, Space geodetic measurement of crustal deformation in central and southern California, 1984-1992, *J. Geophys. Res., 98,* 21,677–21,712, 1993.

Herring, T. A. , GLOBK: Global Kalman filter VLBI and GPS analysis program, Technical report, Massachusetts Institute of Technology, Cambridge, MA, 1995.

Hudnut, K. W. , Y. Bock, M. Cline, P. Fang, J. Freymueller, K. Gross, D. Jackson, S. Larsen, M. Lisowski, Z. Shen, and J. Svarc, Coseismic displacements in the 1992 Landers earthquake sequence, *Bull. Seis. Soc. Am., 84,* 625–645, 1994.

King, R. W. and Y. Bock, Documentation for the MIT GPS analysis software: GAMIT, Technical report, Massachusetts Institute of Technology, Cambridge, MA, 1995.

Reheis, M. C. and T. L. Sawyer, Late Cenozoic history and slip rates of the Fish Lake Valley, Emigrant Peak, and Deep Springs fault zones, Nevada and California, *Geol. Soc. Am. Bull., 109,* 280–299, 1997.

Sauber, J. , W. Thatcher, S. Solomon, and M. Lisowski, Geodetic slip rate for the eastern California shear zone and the recurrence time of Mojave desert earthquakes, *Nature, 367,* 264–266, 1994.

Savage, J. C. and M. Lisowski, Strain accumulation in Owens Valley, California, *Bull. Seis. Soc. Am., 85,* 151–158, 1995.

Savage, J. C. , M. Lisowski, W. K. Gross, N. E. King, and J. L. Svarc, Strain accumulation near Yucca Mountain, Nevada, 1983-1993, *J. Geophys. Res., 99,* 18,103–18,107, 1994.

Wernicke, B. , G. J. Axen, and J. K. Snow, Basin and Range extensional tectonics at the latitude of Las Vegas, Nevada, *Geol. Soc. Am. Bull., 100,* 1738–1757, 1988.

Zhang, P. M. , D. Ellis, D. Slemmons, and F. Mao, Right-lateral displacements and Holocene rate associated with prehistoric earthquakes along the southern Panamint Valley fault zone, *J. Geophys. Res., 95,* 4857–4872, 1990.

This manuscript was prepared with the AGU LaTeX macros v3.1.

Figure 1. General location map showing major fault zones of California and Nevada. Sites of our GPS network are indicated by black triangles. Small boxes show the locations of subnetworks. The larger box shows the location of Figures 2 and 3. The relative velocity between sites MOJA and VNDN (38.5 ± 0.2 mm/yr, 318°, one standard deviation) is indicated by the arrow at site VNDN. The velocity of site MOJA with respect to North America (8.4 ± 0.2 mm/yr, 333°) is not shown. DVFC, HMPV, and OVFZ indicate the locations of the Death Valley-Furnace Creek, Hunter Mountain-Panamint Valley, and Owens Valley fault zones. Diamonds show the locations of the 1992 M_s 7.5 Landers (CA) and M_s 5.4 Little Skull Mountain (NV) earthquakes.

Figure 2. Velocity estimates from five years (1991, 1993, 1994, 1995, 1996) of GPS observations computed with respect to site BLC1. Error ellipses represent the 95% confidence level. The GPS network covers a portion of the eastern California shear zone (ECSZ). The dark sinuous lines represent faults; the dashed northwest trending straight line represents the California-Nevada border. Deformation recorded by these data is dominated by right-lateral shear centered on the Death Valley fault.

Figure 3. Time series for the motion of site LEEF with respect to BLC1. The baseline crosses the breadth of the network. The velocity estimates for the baseline components are (a) north, 3.6 ± 0.4 mm/yr; (b) east, -1.8 ± 0.4 mm/yr; (c) up, 0 ± 2.

Figure 4. Residual velocities after removing the effects of an elastic block model representing the Death Valley-Furnace Creek (DVFC), and Hunter Mountain-Panamint Valley (HMPV) faults. Model faults are indicated by dark solid lines. The fault slip rates were inferred by a least squares fit to the GPS velocity estimates. We estimate a sum of right-lateral slip rates across the two fault systems of 5 ± 1 mm/yr, all of which could be accommodated by the DVFC fault zone. Error ellipses represent the 95% confidence level with respect to a no net translation reference frame. Sites AUGE, DANT, and DS10 were not used in determining the fault slip rates.

Table 1. GPS Site Velocities

Site	Lon. (deg)	Lat. (deg)	East (mm/yr)	North (mm/yr)	ρ	Up (mm/yr)
67TJ	243.6	36.8	-0.2 ± 0.3	-0.4 ± 0.3	-0.027	-3 ± 2
AGUE	242.9	36.4	1.9 ± 0.5	3.6 ± 0.5	-0.033	0 ± 3
BLC1	243.4	36.8	0.0 ± 0.0	0.0 ± 0.0	0.000	0 ± 0
CLAI	243.3	36.9	-1.2 ± 0.3	0.1 ± 0.3	-0.004	-2 ± 2
DANT	243.3	36.2	0.0 ± 0.5	-1.4 ± 0.4	0.057	10 ± 3
FLAT	242.4	36.5	-3.0 ± 0.4	2.5 ± 0.4	-0.052	-4 ± 3
GRAP	242.6	37.9	1.0 ± 0.6	0.3 ± 0.5	-0.035	-9 ± 4
HUNT	242.5	36.6	-1.1 ± 0.4	3.8 ± 0.4	-0.026	-4 ± 3
JACK	242.5	36.5	-2.0 ± 0.4	2.7 ± 0.4	-0.013	-3 ± 3
LEEF	242.4	36.5	-1.8 ± 0.4	3.6 ± 0.4	0.030	0 ± 2
MILE	243.5	36.8	-0.7 ± 0.3	-0.5 ± 0.3	-0.029	-4 ± 2
NEV1	242.7	37.1	0.2 ± 0.4	0.9 ± 0.3	0.002	-2 ± 2
SND1	242.6	37.0	-1.0 ± 0.5	1.7 ± 0.4	-0.072	-2 ± 3
TINP	242.5	36.7	-1.0 ± 0.5	2.0 ± 0.4	-0.077	-1 ± 3
WAHO	243.7	36.8	0.1 ± 0.3	-1.4 ± 0.3	-0.041	-6 ± 2

ρ = correlation coefficient between north and east velocity estimates. Velocities are relative to site BLC1. Errors represent one standard deviation.

Table 2. Fault Slip Rate Estimates (mm/yr)

No.	DVFC	HMPV	OVFZ	DV+HM	χ^2	SL
1	3 ± 2	3 ± 3	-8 ± 24	6 ± 2	124	-
2	3 ± 2	2 ± 3	0	5 ± 2	126	39%
3	4 ± 2	2 ± 3	7	5 ± 2	128	52%
4	5 ± 1	0	4 ± 20	5 ± 1	126	33%
5	0 ± 0	7 ± 2	-27 ± 24	7 ± 2	160	98%
6	5 ± 1	0	0	5 ± 1	126	0%
7	3 ± 1	2 ± 2	1 ± 2	5 ± 1	126	-

DVFC = Death Valley-Furnace Creek fault slip rate. HMPV = Hunter Mountain-Panamint Valley fault slip rate. OVFZ = Owens Valley fault slip rate. DV+HM = sum of DVFC and HMPV estimates. χ^2 = chi-square value. SL = significance level with which we may reject this solution in favor of solution 1. All fault slip rates were estimated without *a priori* constraints with the following two exceptions: (1) Those rates for which no standard error is shown are fixed to this value. (2) For solution 7, HMPV and OVFZ were constrained to their paleoseismological values (see text). Errors represent one standard deviation.

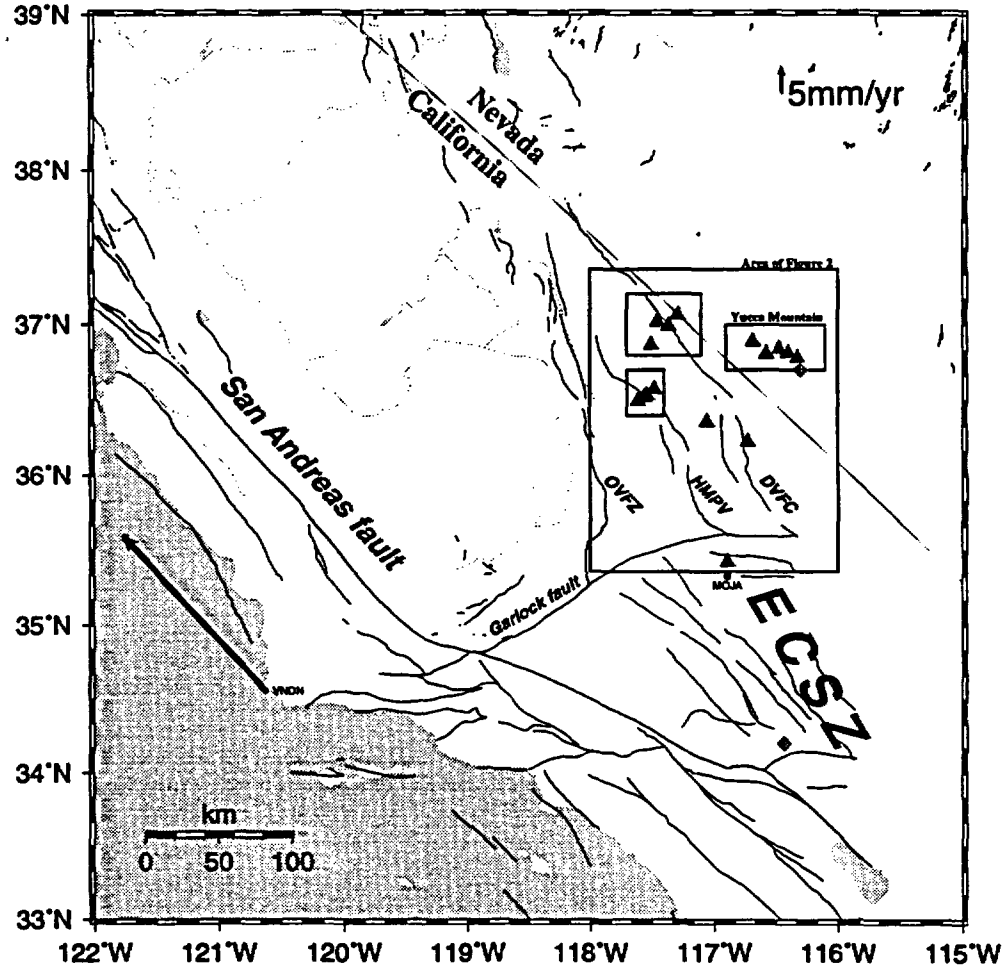
39°N
38°N
37°N
36°N
35°N
34°N
33°N
122°W
121°W
120°W
119°W
118°W
117°W
116°W
115°W
5mm/yr
Nevada
California
San Andreas fault
Garlock fault
Area of Figure 2
Yucca Mountain
OVFZ
HMPV
DVFC
MOJA
YNDN
ECSZ
km
0
50
100

Figure 1.

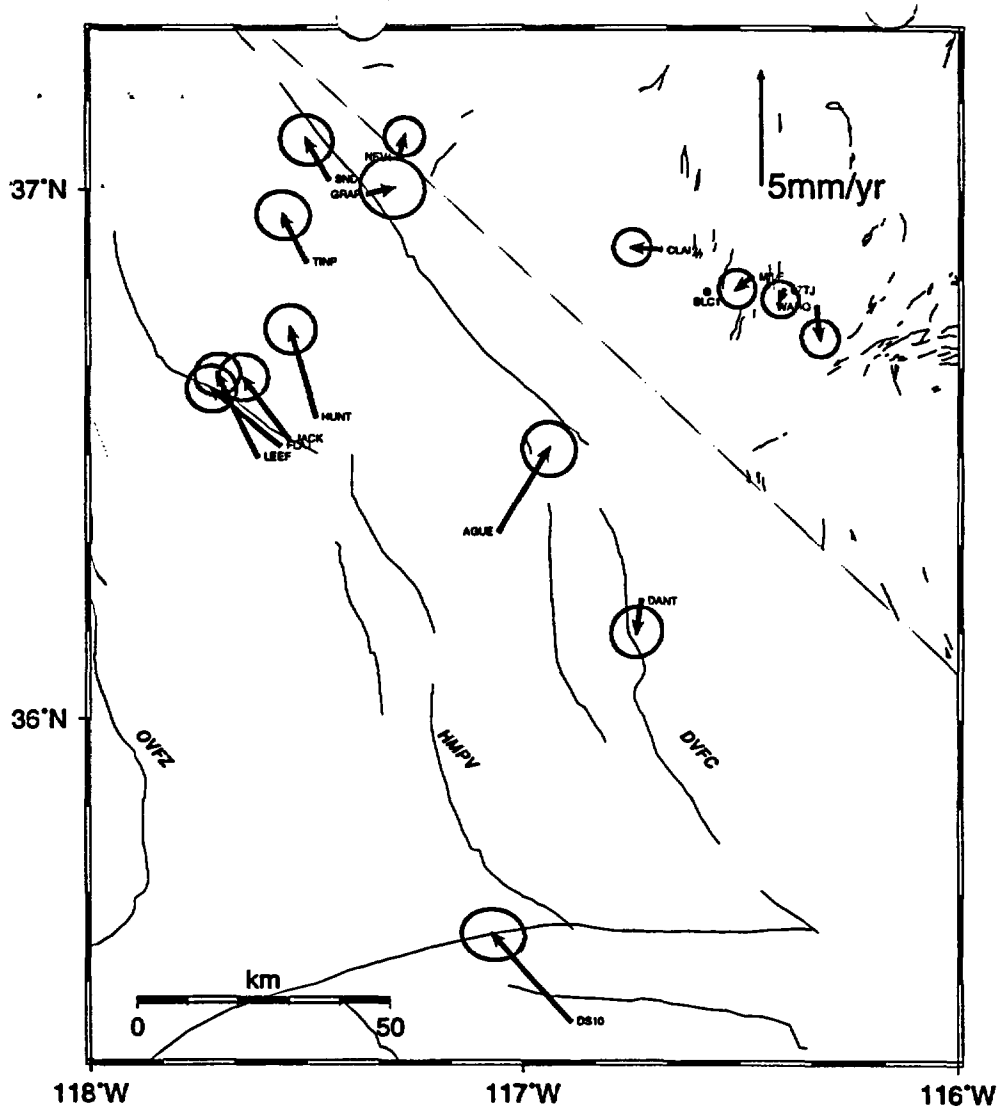
37°N
36°N
118°W
117°W
116°W
5mm/yr
TINP
HUNT
JACK
FOLK
LEEF
AGUE
DANT
DS10
OVFZ
HMPV
DVFC
km
0
50

Figure 2.

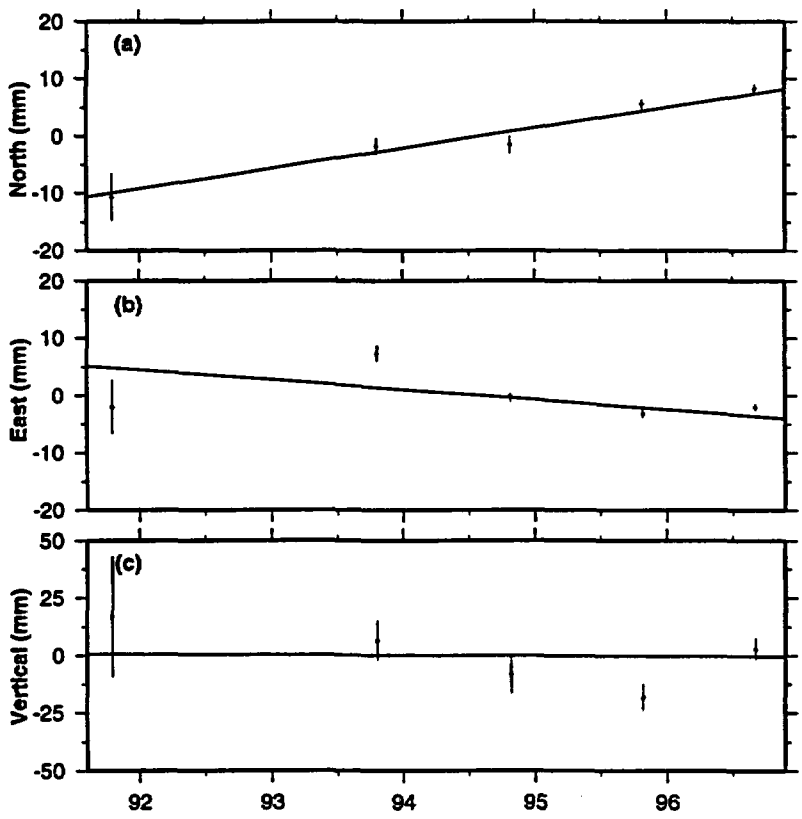
(a)
North (mm)
20
10
0
-10
-20
(b)
East (mm)
20
10
0
-10
-20
(c)
Vertical (mm)
50
25
0
-25
-50
92
93
94
95
96

Figure 3.

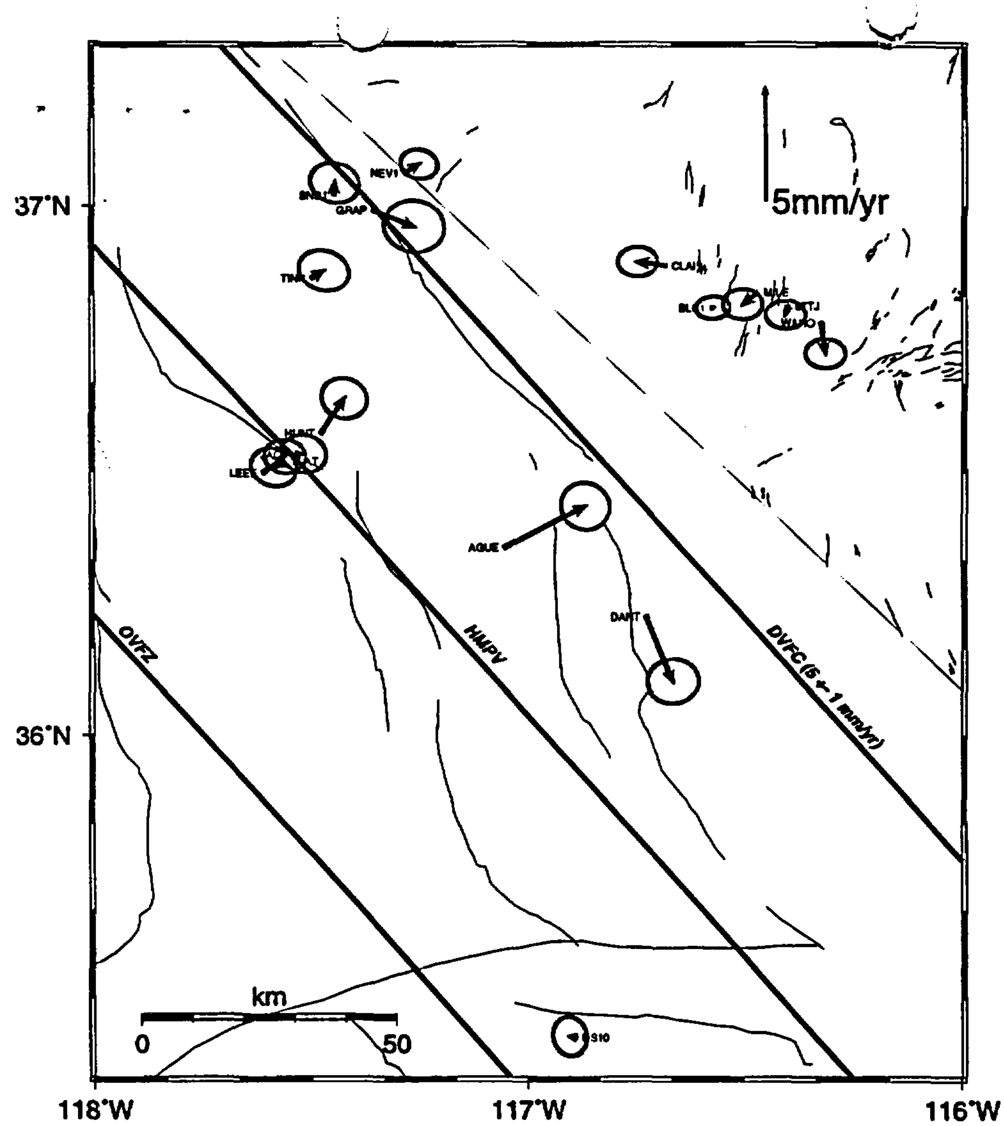
5mm/yr
NEV1
GRAP
TIN
CLAI
AGUE
DART
S10
OVFZ
HMPV
DVFC (5 +- 1 mm/yr)
37°N
36°N
km
0
50
118°W
117°W
116°W

Figure 4.